Polymer Journal

REGULAR ARTICLE

Composition Dependence of Crystallization Behavior Observed in Crystalline-Crystalline Diblock Copolymers

*By Hiroshi IKEDA, Yuya OHGUMA, and Shuichi NOJIMA**

The crystallization behavior of poly(ε-caprolactone) (PCL) blocks starting from a solid morphology formed in advance by the crystallization of polyethylene (PE) blocks (PE-crystallized morphology) in PCL-*b*-PE diblock copolymers has been investigated by a time-resolved synchrotron small-angle X-ray scattering (SR-SAXS) method as a function of composition (or volume fraction of PE blocks ϕ_{PE} in the system). The PE-crystallized morphology and the crystallized state of PCL blocks (*i.e.*, melting temperature and crystallinity of PCL blocks) were examined by static SAXS and differential scanning calorimetry methods, respectively. When PCL-*b*-PE with $\phi_{PE} \leq 0.58$ was quenched from a microphase-separated melt into low temperatures T_c ($30\,^\circ C \leq T_c \leq 45\,^\circ C$), the PE block crystallized first to yield the PE lamellar morphology, an alternating structure consisting of thin PE crystals and amorphous PE + PCL layers, followed by the crystallization of PCL blocks starting from this PE lamellar morphology, where two different crystallization behaviors of PCL blocks were observed depending on T_c; at higher T_c ($\geq 40\,^\circ C$) the Avrami index was *ca.* 3, indicating a heterogeneous crystallization in 3D space. However, it was smaller (~ 2) at lower T_c ($\leq 38\,^\circ C$), suggesting a confined crystallization within the PE lamellar morphology. The temperature at which the crystallization mechanism changed was almost independent of ϕ_{PE} in these copolymers. The late stage of PCL crystallization (or post-Avrami process) was not significantly dependent on ϕ_{PE} and similar to that of crystalline homopolymers. For PCL-*b*-PE with $\phi_{PE} \geq 0.73$, the PE block crystallized on the basis of molten microdomains to yield the PE-crystallized microdomain, and eventually PCL crystallization was confined within this microdomain for every T_c at early and late stages. These results were consistent with our previous conclusions derived from the investigation of resulting morphology.

KEY WORDS: Crystalline-Crystalline Diblock Copolymer / Composition / Crystallization Behavior / Synchrotron SAXS /

Crystalline-crystalline diblock copolymers show a complicated morphology formation according to the melting temperature T_m of constituent blocks when they are quenched from a microphase-separated melt into low temperatures.[1] If T_m values of two blocks are close enough, we have a simultaneous crystallization of both blocks to result in a complicated morphology formation.[2–8] If T_m of one block is enough higher than that of the other, we have a two-step crystallization; high-T_m blocks crystallize first to form a crystallized morphology and subsequently low-T_m blocks start to crystallize from this morphology. Therefore the crystallized morphology formed by high-T_m blocks is a kind of spatial confinement for the subsequent crystallization of low-T_m blocks, which will be qualitatively different from the confinement imposed by amorphous or glassy microdomains observed in crystalline-amorphous diblock copolymers.[9–11] There are some studies so far on the morphology formation of double crystalline block copolymers with different T_m values,[12–24] where they are mainly focused on the characteristic morphology finally formed in the system.

We have recently studied the crystallization behavior and resulting morphology of poly(ε-caprolactone)-*block*-polyethylene (PCL-*b*-PE) diblock copolymers,[25,26] where T_m of PCL blocks was *ca.* 60 °C and that of PE blocks *ca.* 100 °C, so that PE blocks crystallized first by quenching followed by the crystallization of PCL blocks. It was found from these studies that the crystallization behavior of PCL blocks and also resulting morphology were significantly influenced by the crystallization temperature of PCL blocks T_c; at lower T_c ($< 30\,^\circ C$), PCL blocks crystallized within the existing PE lamellar morphology (an alternating structure consisting of thin PE crystals and amorphous PE + PCL layers) as a template, while at higher T_c ($> 35\,^\circ C$) it crystallized by deforming and/or partially destroying the PE lamellar morphology. As a result, the final morphology depended intimately on T_c, and the transition temperature T_p was 30–40 °C for selected PCL-*b*-PE copolymers.

Recently we further investigated the composition (or volume fraction of PE blocks ϕ_{PE} in the system) dependence of resulting morphology mainly by a static small-angle X-ray scattering (SAXS) technique,[27] and found that T_p was *ca.* 33 °C and almost independent of ϕ_{PE} when ϕ_{PE} was not close to 1. This fact suggests that the existing PE lamellar morphology works as a combined confinement of rubbery and glassy microdomains against the crystallization of PCL blocks. That is, the PE lamellar morphology acts as a glassy confinement at lower T_c and as a rubbery confinement at higher T_c, where a competition is expected at each T_c between morphological transition by the crystallization of PCL blocks and suppression of this transition by the PE lamellar morphology.

Department of Organic and Polymeric Materials, Graduate School of Science and Engineering, Tokyo Institute of Technology, H-125, 2-12-1 Ookayama, Meguro-Ku, Tokyo 152-8552, Japan
*To whom correspondence should be addressed (Tel: +81-3-5734-2132, Fax: +81-3-5734-2888, E-mail: snojima@polymer.titech.ac.jp).

In this study, we quantitatively analyze the crystallization behavior of PCL blocks by using a time-resolved synchrotron SAXS method, and try to understand the morphology formation at each T_c as a function of ϕ_{PE}. From these results, we aim to evaluate the composition dependence of the crystallization behavior of PCL blocks observed in PCL-*b*-PE copolymers.

EXPERIMENTAL

Samples

Samples used in this study were poly(ε-caprolactone)-*block*-polyethylene (PCL-*b*-PE) diblock copolymers with varying compositions, which were identical copolymers we used in static measurements,[27] and denoted as E86, E73, E58, E49, E36, E31, and E25, where the numeral represents the volume % of PE blocks in PCL-*b*-PE (see Table I of ref. 27). The melting temperature of PE blocks was *ca.* 100 °C and that of PCL blocks *ca.* 60 °C, so that PE blocks crystallized first by quenching from a microphase-separated melt into low T_c ($\leq$ 45 °C) to yield the PE-crystallized morphology followed by the crystallization of PCL blocks.

The crystallinity of PE blocks in the system χ_{PE} changed from 0.02 to 0.19 (or crystallinity of PE blocks in the whole PE blocks from 0.06 to 0.23), and therefore we can expect a wide variation in constraint strength by the PE-crystallized morphology against PCL crystallization. In addition, the PE-crystallized morphology depended intimately on ϕ_{PE}, which will be described in Results and Discussion.

Differential Scanning Calorimetry (DSC) Measurements

A Perkin Elmer DSC Pyris 1 was used to investigate the melting temperature and crystallinity of PCL blocks to understand the crystallized PCL state. First, samples were cooled at 10 °C/min from a microphase-separated melt into 0 °C to obtain an exothermic peak owing to the non-isothermal crystallization of PCL blocks, annealed at 0 °C for 5 min, and finally heated at 10 °C/min, where we observed an endothermic peak due to the melting of PCL blocks. The crystallinity of PCL blocks on cooling χ_{PCL} or on heating χ'_{PCL} was calculated by assuming that the exothermic heat flow to form (or the heat of fusion for) perfect PCL crystals was 135.44 J/g.[28]

Synchrotron Small-Angle X-ray Scattering (SR-SAXS) Measurements

Microphase-separated samples at 120 °C were quenched into each T_c, and the isothermal crystallization process of PCL blocks was pursued by a time-resolved SR-SAXS technique.

The SR-SAXS measurement was performed at Photon Factory in high-energy accelerator research organization, Tsukuba Japan, with a small-angle X-ray equipment for solution (SAXES) installed at beam line BL-10C. Details of the equipment and the intensity correction procedure were already described elsewhere.[29–31] Accumulation time for each frame was 10 s, and the measurement was continued until an integrated intensity did not change any more. The SAXS curves were finally obtained as a function of $s = (2/\lambda)\sin\theta$, where λ is the wavelength of incident X-ray (= 0.1488 nm) and 2θ the scattering angle. Parameters characterizing the crystallization behavior of PCL blocks were finally extracted from these SAXS curves as a function of crystallization time t_c.

Conventional Small-Angle X-ray Scattering (C-SAXS) Measurements

C-SAXS measurements were performed by using a Rigaku Nano-Viewer with a rotating-anode X-ray generator operating at 45 kV and 60 mA. The detector was a one-dimensional position-sensitive proportional counter (PSPC), and accumulation time for each measurement was 1 h. Methods of data treatment were the same to that of the SR-SAXS measurement.

Analysis of Time-resolved SR-SAXS Curves

Decomposition of SAXS Peaks. The SR-SAXS curves have an intensity peak arising from the PE lamellar morphology, and another intensity peak appears at lower angle with increasing t_c for PCL-*b*-PE crystallized at higher T_c ($\geq$ 40 °C), which comes from the PCL lamellar morphology (an alternating structure consisting of PCL crystals and combined layers of amorphous PE + PCL and crystallized PE) gradually formed in the system. Therefore, peak decomposition is necessary to discuss the crystallization behavior of PCL blocks at higher T_c though the angular positions of two intensity peaks are very close to each other.

We assume that the scattered intensity $I(t_c, s)$ at t_c is a combination of those at $t_c = 0$ (arising from the PE lamellar morphology) and $t_c = \infty$ (from the PCL lamellar morphology), and then we can describe,

$$I(t_c, s) = A(t_c)I(0, s) + B(t_c)I(\infty, s) \quad (1)$$

where $A(t_c)$ and $B(t_c)$ represent the contribution of each scattered intensity at t_c assuming they are independent of s, and $A(0) = 1$, $B(0) = 0$, $A(\infty) = 0$, and $B(\infty) = 1$. By defining $s_{1,max}$ as the angular position of intensity peak from the PE lamellar morphology and $s_{2,max}$ that from the PCL lamellar morphology, we obtain,

$$I(t_c, s_{1,max}) = A(t_c)I(0, s_{1,max}) + B(t_c)I(\infty, s_{1,max}) \quad (2)$$

$$I(t_c, s_{2,max}) = A(t_c)I(0, s_{2,max}) + B(t_c)I(\infty, s_{2,max}) \quad (3)$$

By solving above simultaneous equations we can evaluate $A(t_c)$ and $B(t_c)$ as a function of t_c. It should be noted that this treatment is only valid for higher T_c, where the pre-existing PE lamellar morphology is completely replaced with the PCL lamellar morphology at $t = \infty$. That is, at lower T_c ($\leq$ 38 °C), $A(\infty) = 0$ does not hold because the PE lamellar morphology remains in the system at $t = \infty$ owing to the confined crystallization of PCL blocks within it. In such a case, we simply approximate the intensity peak by a single function to get the t_c dependence of peak intensity.

Analysis for Early Stage Crystallization. The early stage of crystallization is analyzed by using Avrami equation,[32] which is widely used for the analysis of early stage crystallization of homopolymers. The volume fraction $X(t_c)$ of crystals existing in the system at t_c is given by,

$$X(t_c) = 1 - \exp[-(Kt_c)^n] \quad (4)$$

where K is a rate constant and n is the Avrami index expressing the mode of crystallization. $X(t_c)$ is normalized so as to take unity at $t_c = \infty$ for polymer systems. The invariant (or integrated intensity) $Q(t_c)$ or the maximum of intensity peak $I_{max}(t_c)$ from lamellar morphology was usually used as $X(t_c)$ for the analysis of SR-SAXS curves assuming that the alternating structure does not change within crystallized regions during early stage crystallization. After normalizing $I_{max}(t_c)$ by the final value $I_{max}(\infty)$, we obtain,

$$X(t_c) = I_{max}(t_c)/I_{max}(\infty) \quad (5)$$

Equation (4) is then reduced to

$$\log\{-\ln[1 - I_{max}(t_c)/I_{max}(\infty)]\} = n(\log t_c + \log K) \quad (6)$$

It is possible to evaluate n and K from the plot of $\log\{-\ln[1 - I_{max}(t_c)/I_{max}(\infty)]\}$ against $\log t_c$.

Analysis for Late Stage Crystallization. Many methods are proposed to quantitatively describe the late stage crystallization (or post-Avrami process) of homopolymers, and they consist of first-order process as,

$$X(t_c) = 1 - \exp\{-K'(t_c - \tau)\} \quad (7)$$

where K' is the rate constant of this stage and τ is the time at which this stage starts. Equation (7) has been applied for many homopolymers so far, and found to adequately describe the late stage crystallization of homopolymers and block copolymers.[33–35] We apply equation (7) for our systems at $0.5 < I_{max}(t_c)/I_{max}(\infty) < 0.9$, and evaluate K' and τ by plotting $\ln[1 - X(t_c)]$ against t_c with $X(t_c)$ given by eq. (5).

Next we consider a dimensionless parameter θ defined by,

$$\theta = K'/K \quad (8)$$

θ represents the ratio of crystallization rates at early and late stages, and depends significantly on total crystallization behavior at T_c.[35] For example, θ becomes smaller when the late stage crystallization proceeds more slowly with a same crystallization rate at early stage. Therefore, θ gives quantitative information on relative rates of early and late stage crystallizations when the total crystallization process is compared among different conditions.

RESULTS AND DISCUSSION

PE-crystallized Morphology

When PCL-*b*-PE copolymers are quenched from a microphase-separated melt into low T_c, PE blocks crystallize first to form the PE-crystallized morphology followed by the crystallization of PCL blocks starting from this morphology. Therefore it is important to quantitatively understand the PE-crystallized morphology as a function of ϕ_{PE} in order to discuss the crystallization behavior of PCL blocks.

Figure 1 shows the long period (LP), an alternating distance of the structure formed, plotted against temperature for E49 (a) and E73 (b), where the closed circle indicates the results above

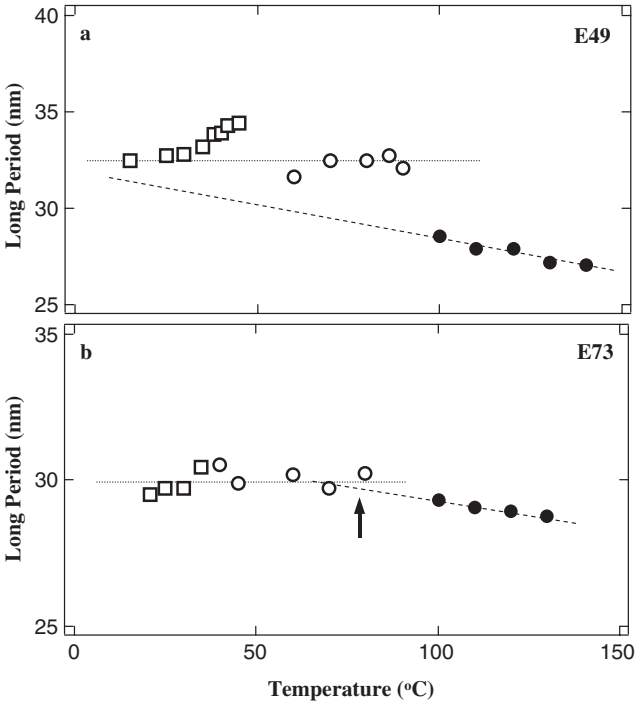

Figure 1. Long period plotted against temperature for E49 (a) and E73 (b). ●: Both PE and PCL amorphous. ○: PE crystallized and PCL amorphous. □: Both PE and PCL crystallized.

the melting temperature of both blocks and hence represents LP of the microdomain structure. Open circle and square indicate results at lower temperatures and represent LP of the PE-crystallized morphology and PE + PCL-crystallized morphology, respectively. LP of the microdomain structure increases steadily with decreasing temperature for both copolymers, and this result arises from several factors such as the change in block incompatibility and chain conformation.[36] However the extrapolated LP for E49 is significantly smaller than that for the PE- (and also PE + PCL-) crystallized morphology, and it increases discontinuously by the crystallization of PE blocks, indicating that the morphology after PE crystallization is not based on the microdomain structure, *i.e.*, a morphological transition occurs from the microdomain structure into the PE lamellar morphology.[29] Figure 1a is qualitatively similar to the result reported by Register *et al.* for a break-out crystallization observed in PE-*block*-poly(3-methyl-1-butene) copolymers.[37] We obtained same results for E25, E31, E36, and E58.

The morphology formed in E73 (and also E86) by the crystallization of PE blocks, on the other hand, seems to be frozen with LP exactly corresponding to that of the microdomain structure existing just before the crystallization (shown by an arrow in Figure 1b). This fact suggests that the microdomain structure holds even after PE crystallization, that is, PE blocks crystallize within the molten microdomain structure. The rapid crystallization of PE blocks may be responsible for this confined crystallization because the total molecular weight of E73 and E86 is not large enough

($M_n = 14{,}000$–$16{,}000$) and accordingly the microdomain structure itself will not be stable against the subsequent crystallization of PE blocks. This confined crystallization is sometimes reported for PE-containing crystalline-amorphous diblock copolymers with a relatively low molecular weight.[37]

In summary, judging from the temperature dependence of LP, we have two types of PE-crystallized morphology depending on ϕ_{PE} just before the crystallization of PCL blocks; we have the PE lamellar morphology for E25, E31, E36, E49, and E58 while the PE-crystallized microdomain for E73 and E86. In the latter case, the matrix is composed of PE blocks, so that the crystallization of PE blocks also leads to the PE lamellar morphology though amorphous PCL regions are cylindrically isolated within this PE lamellar morphology, which is substantially different from the former case; amorphous PCL regions are sandwiched between amorphous and crystallized PE layers. However, it will be true for both cases that the crystallization of PCL blocks will be significantly restricted through the existing PE lamellar crystals.

In order to check the substantial difference in the final crystallized state of PCL blocks between two cases, we measured the crystallinity χ_{PCL} of PCL blocks during cooling at 10 °C/min and the melting temperature $T_{m,PCL}$ during heating at 10 °C/min as a function of ϕ_{PE}. They are plotted in Figure 2, where χ_{PCL} and $T_{m,PCL}$ for a PCL homopolymer ($M_n = 7{,}700$ and $M_w/M_n = 1.16$) are added for comparison (closed symbols). $T_{m,PCL}$ is intimately related to the size of PCL crystals and χ_{PCL} the degree of interference by existing PE crystals when PCL blocks crystallize, and therefore they are a measure for crystallizability of PCL blocks in different conditions. χ_{PCL} and $T_{m,PCL}$ for E73 and E86 are slightly lower than those of other copolymers and also the PCL homopolymer but the difference is moderately small when compared with completely confined crystallization observed in high-molecular weight crystalline-amorphous diblock copolymers, where the crystallinity and melting temperature reduce considerably in case of spherical or cylindrical confinement.[38,39] Figure 2 suggests that the final crystallized PCL state does not depend critically on the amorphous PCL state just before the crystallization. Therefore we hereafter consider the effect of the PE lamellar morphology on the crystallization behavior of PCL blocks for PCL-*b*-PE copolymers all together with paying attention to a small difference in the amorphous PCL state.

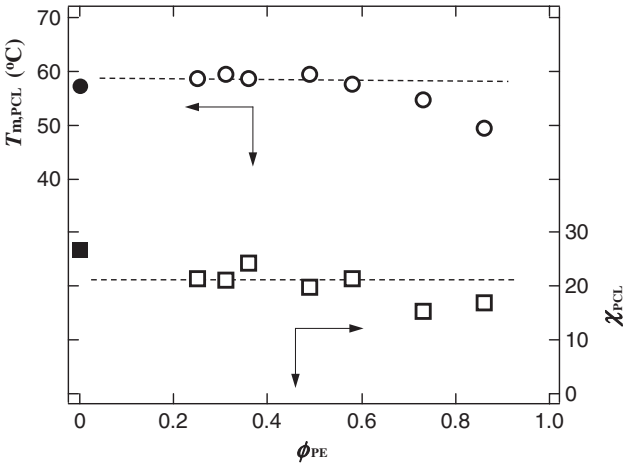

Figure 2. χ_{PCL} and $T_{m,PCL}$ plotted against ϕ_{PE} for all PCL-*b*-PE copolymers investigated. χ_{PCL} was obtained during cooling at 10 °C/min, and $T_{m,PCL}$ during heating at 10 °C/min for the samples crystallized at 0 °C for 5 min. Closed symbols represent the results of a PCL homopolymer ($M_n = 7{,}700$ and $M_w/M_n = 1.16$).

SR-SAXS Results for the Crystallization Process of PCL Blocks

Figure 3 shows typical SR-SAXS curves after quenching E31 from 120 °C (*i.e.*, from microphase-separated melt) into 42 °C (a) and E73 into 20 °C (b), where we mainly observe the crystallization process of PCL blocks. In Figure 3a, a sharp diffraction arising from a microdomain structure (at $t_c = 5$ s) turns quickly into a small scattered peak with a considerable shift of peak position to lower angle, indicating that the microdomain structure is completely transformed into the PE lamellar morphology by the crystallization of PE blocks. After

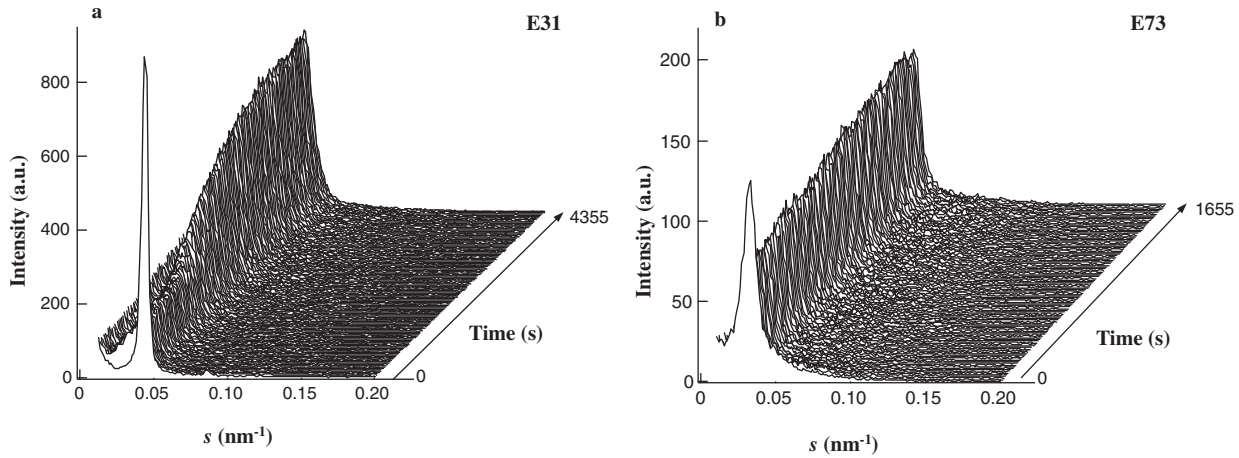

Figure 3. Typical SR-SAXS curves during isothermal crystallization for E31 at 42 °C (a) and E73 at 20 °C (b).

some induction time, the peak intensity gradually increases and simultaneously the peak position moves slightly to lower angle with increasing t_c, which arises from the crystallization of PCL blocks starting from the PE lamellar morphology. This shift of peak position can not be observed at lower T_c ($< 30\,^\circ$C), because PCL blocks crystallize within the existing PE lamellar morphology.[26] In Figure 3b, SR-SAXS curves are largely different from those in Figure 3a. The crystallization of PE blocks is extremely fast and finished substantially during quenching without any change of peak position. That is, only first large peak (at $t_c = 5$ s) arises from a transient morphology during PE crystallization and after that no indication of further PE crystallization is observed. With increasing t_c the peak intensity increases slightly by the crystallization of PCL blocks, but the peak position does not move at all through the crystallization process of PCL blocks. Note that we could not observe the crystallization process of PCL blocks in E73 and E86 at higher T_c ($\geq 22\,^\circ$C) because it took too long time to be pursued by the SR-SAXS method.

In our previous studies,[25,26] we demonstrated that the peak shift observed in Figure 3a during PCL crystallization at higher T_c ($\geq 40\,^\circ$C) resulted from the superposition of two scattering peaks; one at higher-angle arises from the PE lamellar morphology and the other at lower-angle from the PCL lamellar morphology newly formed in the system, and the higher-angle peak is gradually replaced with the lower-angle peak as PCL blocks crystallize. Therefore it is necessary for this case (*i.e.*, higher T_c) to make peak decomposition in order to analyze the crystallization behavior of PCL blocks separately.

Figure 4a shows the peak intensity plotted against t_c for E49 crystallized at 42 °C (higher T_c) when the scattered peak is approximated by a single parabolic function because at a first glance the intensity peak seems to change continuously with t_c. But this treatment is not logically correct as described above, and also we observe a bimodal intensity peak at selected t_c (for example, see Figure 5 of ref. 26). Figure 4b shows results after peak decomposition by using eqs. 2 and 3, where data points are considerably scattered because they are evaluated from the intensities only at $s_{1,max}$ and $s_{2,max}$, and no smoothing process is included in the calculation procedure. The peak intensity from the PCL lamellar morphology (○), which is a measure for the development of PCL crystallization, increases roughly with a sigmoid shape and simultaneously the peak intensity from the PE lamellar morphology (△) decays and finally disappears. From this t_c dependence of the increasing peak intensity, it is possible to analyze the early and late stages of PCL crystallization at higher T_c. On the other hand, we approximated the scattered peak by a single function for lower T_c ($\leq 38\,^\circ$C), and the increasing intensity was used to analyze the crystallization process of PCL blocks.

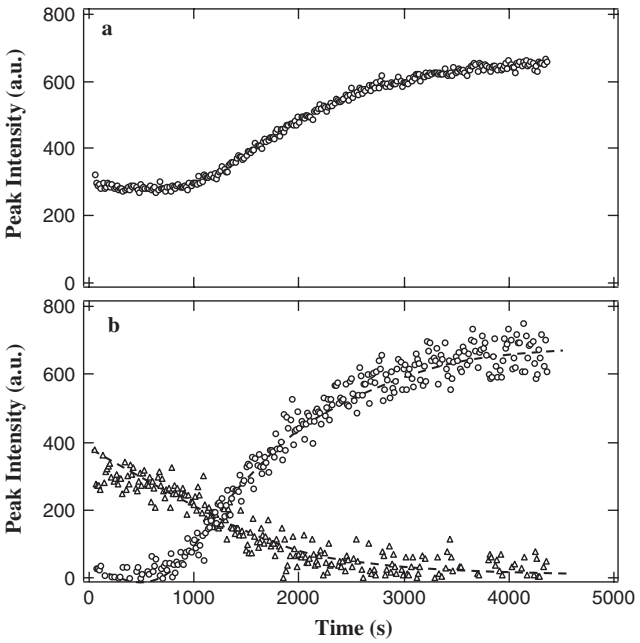

Figure 4. Peak intensities plotted against t_c for E49 crystallized at 42 °C. The scattered peak is approximated by a single parabolic function (a) and the peak is decomposed into two by the method shown in the text (b). ○: Peak intensity from the PCL lamellar morphology. △: Peak intensity from the PE lamellar morphology.

Analysis for Early Stage Crystallization of PCL Blocks

Figure 5 shows an example of Avrami plots for E25 crystallized at 41 °C (○) and E73 at 20 °C (□), where we have a linear relationship for both cases with different slopes (*i.e.*, $n \sim 3$ for E25 and $n \sim 2$ for E73). Here, the data for first 25% in intensity are used because the Avrami analysis is valid only for the early stage of crystallization. We had similar plots for every sample at each T_c and could obtain n successfully, though some plots did not have enough data points to determine n unambiguously because the crystallization of PCL blocks was very fast at lower T_c. In such cases, we did not evaluate n.

The values of n are summarized in Figure 6 as a function of T_c for all PCL-*b*-PE copolymers investigated, where closed symbols are derived from the increasing peak intensity after peak decomposition and others obtained by approximating the intensity peak with a single parabolic function. n at higher T_c ($\geq 40\,^\circ$C) is about three, which is usually found in homopolymers and indicates a heterogeneous crystallization in 3D space. This fact suggests that PCL blocks crystallize freely without any constraint by the existing PE lamellar morphology, which is the same conclusion we have previously obtained for selected PCL-*b*-PE copolymers.[26]

The values of n for E73 and E84 and also those for other copolymers at lower T_c ($\leq 38\,^\circ$C) are significantly small ($n \sim 2$), suggesting that the crystallization mechanism is different from that for E25 through E58 at higher T_c ($\geq 40\,^\circ$C). LP after the crystallization of PCL blocks is nearly identical to that of the PE lamellar morphology in these cases, so that we can intuitively suppose that PCL blocks crystallize within the existing PE lamellar morphology. Therefore the crystallization mechanism should be substantially different from that in 3D space. It is already reported that n is extremely reduced when the crystallization is completely restricted within

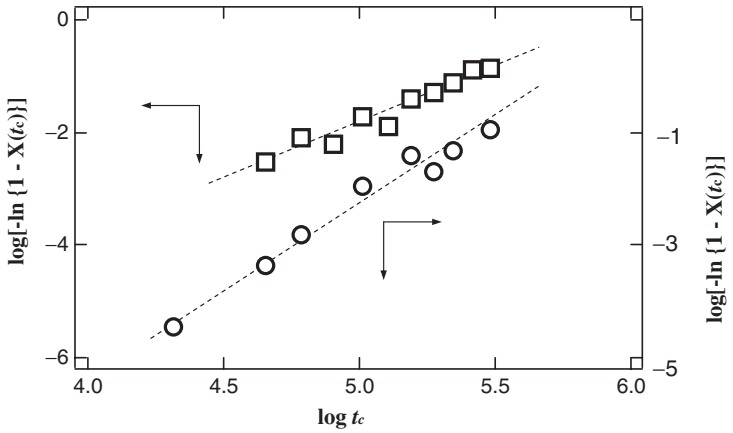

Figure 5. Typical Avrami plots for E25 crystallized at 41 °C (○) and for E73 crystallized at 20 °C (□).

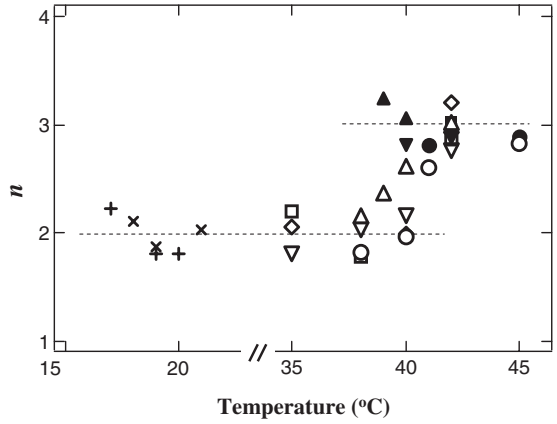

Figure 6. Avrami index n plotted against T_c for E25 (○,●), E31 (□,■), E36 (△,▲), E49 (▽,▼), E58 (◇,◆), E73 (×), and E86 (+). Closed symbols represent the results obtained from the increasing peak intensity after peak decomposition (Figure 4b) and others obtained by approximating the intensity peak with a single parabolic function (Figure 4a).

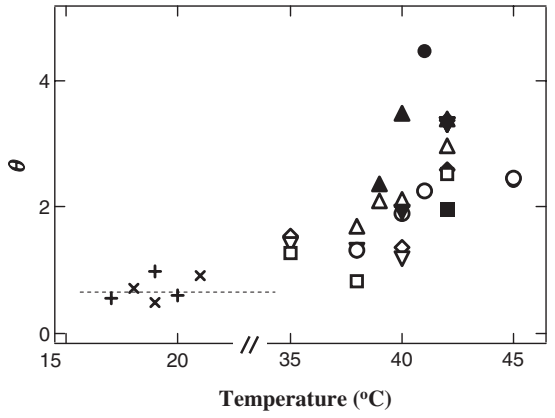

Figure 7. θ plotted against T_c. The symbols are the same with those in Figure 6.

spherical or cylindrical microdomains,[10] and smaller n seems to be characteristic of the confined crystallization.

It is interesting to compare n derived from the peak intensity after peak decomposition (closed symbols) and that simply approximated by a single function (open symbols) for same samples at the same T_c. At higher T_c (≥ 42 °C) they coincide completely (for example, ○ and ● at 45 °C or △ and ▲ at 42 °C), indicating that early stage crystallization is completely controlled by the development of the PCL lamellar morphology newly formed. On the other hand, the difference between two results increases significantly with decreasing T_c (for example, △ and ▲ at 40 and 39 °C), suggesting that early stage crystallization moves to a different mechanism, that is, confined crystallization within the PE lamellar morphology. Therefore, we can consider that two mechanisms work simultaneously in the system at an intermediate T_c range, and their contribution changes gradually with changing T_c. Approximating the intensity peak by a single function corresponds to taking an average between two mechanisms, and hence n decreases gradually with decreasing T_c. On the other hand, the peak intensity after peak decomposition exactly corresponds to the development of the PCL lamellar morphology and hence n remains constant (~ 3). Though this peak decomposition procedure is not logically correct when the crystallized PE lamellar morphology remains after PCL crystallization, it will be justified when the volume fraction of the crystallized PE lamellar morphology is small enough.

Analysis for Late Stage Crystallization of PCL Blocks

The late stage crystallization of PCL blocks, together with the early stage crystallization, was quantitatively analyzed by using eq. 7, and we evaluated θ as a function of T_c for each PCL-*b*-PE.

Figure 7 shows θ plotted against T_c for all PCL-*b*-PE copolymers investigated, where data can be divided into two groups; one consists of results for E86 and E73, where θ is extremely small (~ 0.8), and the other those for E25 through E58, where data points are somewhat scattered but significantly larger than those for the former group, and they increase roughly with increasing T_c. The smaller θ indicates that the early stage crystallization is very fast and/or the crystallization rate retards significantly at the late stage. We previously demonstrated that the confined crystallization of PCL blocks

within the PE lamellar morphology was extremely fast at the early stage (*i.e.*, larger K) compared with a break-out crystallization, and it decelerated moderately at the late stage (smaller K').[26] Therefore, θ ($= K'/K$) takes a very small value (~ 0.8) for the completely confined crystallization within the PE lamellar morphology.

The gradual increase of θ with increasing T_c for E25 through E58 can be explained by considering the crystallization mechanism of PCL blocks at early and late stages. At higher T_c ($\geq 41\,^\circ$C) the early stage crystallization is driven by the development of the new PCL lamellar morphology as described previously (smaller K), and the late stage is a process for further development of this PCL lamellar morphology (larger K' compared with completely confined crystallization). Therefore the whole crystallization process is similar to that for crystalline homopolymers and crystalline-amorphous diblock copolymers without any microdomain structure, where θ takes *ca.* 3,[35] which is moderately consistent with results at higher T_c ($\geq 41\,^\circ$C) shown in Figure 7.

The confined crystallization appears at the early stage with decreasing T_c ($\leq 40\,^\circ$C) and competes with the development of the PCL lamellar morphology, and eventually the apparent crystallization rate (or K) gradually increases, because we evaluate a combined crystallization by assuming a single intensity peak, yielding an increasing K with decreasing T_c. The late stage crystallization in this case is considered to be driven by further development of the PCL lamellar morphology, so that K' is comparable to that for the crystallization process at higher T_c (larger K'). As a result, θ takes an intermediate value (~ 1.8) and decreases gradually with decreasing T_c, as shown in Figure 7. However, θ in this temperature range is significantly larger than that for E73 and E86, because K' is substantially different for both cases.

In summary, we can explain a complicated change in θ against T_c shown in Figure 7 by considering the difference in crystallization mechanism of PCL blocks at early and late stages. That is, the completely confined crystallization for E73 and E86 results in low θ (~ 0.8), the combined crystallization at the early stage followed by the development of the PCL lamellar morphology at late stage for E25 through E58 at lower T_c ($\leq 40\,^\circ$C) yields intermediate θ (~ 1.8), and the development of the PCL lamellar morphology in the whole crystallization process at higher T_c ($\geq 41\,^\circ$C) yields large θ (~ 3).

Composition Dependence of T_c-dependent Crystallization Behavior

We finally examine the composition dependence of T_c-dependent crystallization behavior observed at the early stage. The temperature T_p at which n changes discontinuously, *i.e.*, the crystallization mechanism changes from ordinary crystallization ($n \sim 3$) into confined crystallization ($n \sim 2$), is plotted in Figure 8 against ϕ_{PE}, which is proportional to the volume fraction of PE crystals existing in the system and therefore a measure for the constraint strength of the PE lamellar morphology against PCL crystallization. T_p may be evaluated from Figure 7 as a discontinuous point of θ, but it contains much error for getting reliable θ. In Figure 8, we also add results obtained from the T_c dependence of LP derived from static SAXS measurements in our previous study (○).[27]

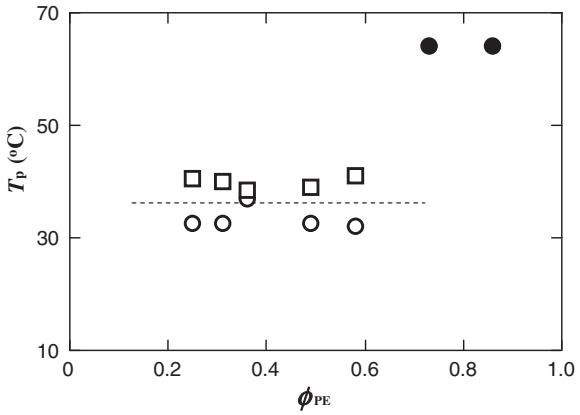

Figure 8. T_p plotted against ϕ_{PE}. □: Derived from Figure 6. ○: Derived from the T_c dependence of LP in our previous study. ●: T_p could not be obtained within our experimentally accessible time, so that we simply assumed $T_p \sim T^0_{m,PCL}$ (equilibrium melting temperature of PCL homopolymer).

We could not observe any change in the crystallization mechanism for E86 and E73 within our experimentally accessible time, which is the same result obtained in our previous study (static SAXS measurements), and therefore we simply put $T_p \sim T^0_{m,PCL}$ in Figure 8, where $T^0_{m,PCL}$ is an equilibrium melting temperature of PCL homopolymers ($\sim 64\,^\circ$C).[40] This fact indicates that the PE lamellar morphology existing in E86 and E73 effectively confines the subsequent crystallization of PCL blocks. On the other hand, T_p values are almost constant ($\sim 39\,^\circ$C) irrespective of composition for E25 through E58, and slightly higher than those obtained by static SAXS measurements ($\sim 33\,^\circ$C), that is, the temperature at which LP deviates significantly from that of the microdomain structure. This difference in T_p might arise from experimental methods employed to evaluate T_p. That is, T_p evaluated in this study reflects the crystallization behavior of PCL blocks only at the early stage while that derived in our previous study is based on the resulting morphology after PCL crystallization has completely finished.

The present results, together with our previous results, indicate that there is a competition between the crystallization of PCL blocks, which facilitates the formation of new morphology, and the constraint by the PE lamellar morphology against morphological rearrangement. Therefore we can understand that the PE lamellar morphology works as an intermediate between rubbery and glassy confinements for the crystallization of PCL blocks, which depends critically on ϕ_{PE} or χ_{PE} (constraint strength by the PE lamellar morphology against PCL crystallization) and T_c (crystallization rate of PCL blocks).

CONCLUSIONS

The crystallization behavior of PCL blocks observed in PCL-*b*-PE copolymers was investigated mainly by a time-

resolved SR-SAXS technique as a function of composition. In these copolymers, PE blocks crystallized first by quenching to form the PE-crystallized morphology, and subsequently the crystallization of PCL blocks started from this morphology. Following conclusions were obtained from this study.

1) When PCL-*b*-PE copolymers with $\phi_{PE} \leq 0.58$ were quenched, we observed two different crystallization behaviors of PCL blocks depending on T_c; at higher T_c ($\geq 40\,^{\circ}C$) the Avrami index n was *ca.* 3, suggesting a heterogeneous crystallization in 3D space, while n was smaller (~ 2) at lower T_c ($\leq 38\,^{\circ}C$), *i.e.*, a significant effect of existing PE crystals on the crystallization behavior of PCL blocks was detected. The gradual decrease in n at around $40\,^{\circ}C$ might arise from the competition of these two mechanisms in the system, and the combined crystallization process was evaluated by the peak intensity analysis to yield the continuous change in n.

2) The temperature T_p at which the crystallization behavior changed in PCL-*b*-PE with $\phi_{PE} \leq 0.58$ was independent of ϕ_{PE}, and nearly identical to that previously derived from the morphological investigation by a static SAXS technique, *i.e.*, the change of LP with T_c.

3) When PCL-*b*-PE copolymers with $\phi_{PE} \geq 0.73$ were quenched from a microphase-separated melt into low T_c ($17\,^{\circ}C \leq T_c \leq 22\,^{\circ}C$), the completely confined crystallization of PE blocks and subsequently that of PCL blocks were observed at every T_c investigated, where n was significantly small (~ 2). The crystallization rate at early stage was fast but that at late stage was slow to result in a very small θ (~ 0.8) compared with other copolymers.

Acknowledgment. This work was supported in part by NEDO (New Energy and Industrial Technology Development Organization) launched in 2001 and also by Grants-in-Aid for Scientific Research on Basic Areas (B) (No. 17350102) from the Ministry of Education, Science, Sports, and Culture of Japan. The SR-SAXS measurement has been performed under the approval of Photon Factory Advisory Committee (No. 2006G078).

Received: October 2, 2007
Accepted: December 1, 2007
Published: January 29, 2008

REFERENCES

1. A. J. Muller, M. L. Arnal, and V. Balsamo, "Lecture Notes in Physics," vol. 714, G. Reiter and G. Strobl, Ed., Springer-Verlag, 2007.
2. S. Nojima, M. Ono, and T. Ashida, *Polym. J.*, **24**, 1271 (1992).
3. Z. Gan, B. Jiang, and J. Zhang, *J. Appl. Polym. Sci.*, **59**, 961 (1996).
4. G. Floudas, G. Reiter, O. Lambert, and P. Dumas, *Macromolecules*, **31**, 7279 (1998).
5. O. Lambert, S. Reutenauer, G. Hurtrez, G. Riess, and P. Dumas, *Polym. Bull.*, **40**, 143 (1998).
6. B. Bogdanov, A. Vidts, E. Schacht, and H. Berghmans, *Macromolecules*, **32**, 726 (1999).
7. T. Shiomi, K. Imai, K. Takenaka, H. Takeshita, H. Hayashi, and Y. Tezuka, *Polymer*, **42**, 3233 (2001).
8. J. Sun, X. Chen, C. He, and X. Jing, *Macromolecules*, **39**, 3717 (2006).
9. S. Nojima, H. Tanaka, A. Rohadi, and S. Sasaki, *Polymer*, **39**, 1727 (1998).
10. Y. L. Loo, R. A. Register, and A. J. Ryan, *Macromolecules*, **35**, 2365 (2002).
11. A. T. Lorenzo, M. L. Arnal, A. J. Muller, A. B. Fierro, and V. Abetz, *Eur. Polym. J.*, **42**, 516 (2006).
12. M. Ueda, K. Sakurai, S. Okamoto, D. J. Lohse, W. J. MacKnight, S. Shinkai, S. Sakurai, and S. Nomura, *Polymer*, **44**, 6995 (2003).
13. J. Albuerne, L. Marquez, A. J. Muller, J. M. Raquez, P. Degee, P. Dubois, V. Castelletto, and I. W. Hamley, *Macromolecules*, **36**, 1633 (2003).
14. R. M. Ho, P. Y. Hsieh, W. H. Tseng, C. C. Lin, B. H. Huang, and B. Lotz, *Macromolecules*, **36**, 9085 (2003).
15. G. Maglio, A. Migliozzi, and R. Palumbo, *Polymer*, **44**, 369 (2003).
16. V. Balsamo, G. Gil, C. U. Navarro, I. W. Hamley, F. Gyldenfeldt, V. Abetz, and E. Canizales, *Macromolecules*, **36**, 4515 (2003).
17. L. Sun, Y. Liu, L. Zhu, B. S. Hsiao, and C. A. Avila-Orta, *Polymer*, **45**, 8181 (2004).
18. P. Huang, L. Zhu, Y. Guo, Q. Ge, A. J. Jing, W. Y. Chen, R. P. Quirk, S. Z. D. Cheng, E. L. Thomas, B. Lotz, B. S. Hsiao, C. A. Avila-Orta, and I. Sic, *Macromolecules*, **37**, 3689 (2004).
19. W. Li, X. Kong, E. Zhou E, and D. Ma, *Polymer*, **46**, 11655 (2005).
20. I. W. Hamley, V. Castelletto, R. V. Castillo, A. J. Muller, C. M. Martin, E. Pollet, and P. Dubois, *Macromolecules*, **38**, 463 (2005).
21. C. P. Radano, O. A. Scherman, N. S. Stutzmann, C. Muller, D. W. Breiby, P. Smith, R. A. J. Janssen, and E. W. Meijer, *J. Am. Chem. Soc.*, **127**, 12502 (2005).
22. I. W. Hamley, P. Parras, V. Castelletto, R. V. Castillo, A. J. Muller, E. Pollet, P. Dubois, and C. M. Martin, *Macromol. Chem. Phys.*, **207**, 941 (2006).
23. J. Yang, T. Zhao, J. Cui, L. Liu, Y. Zhou, G. Li, E. Zhou, and X. Chen, *J. Polym. Sci., Part B: Polym. Phys.*, **44**, 3215 (2006).
24. Y. S. Sun, T. M. Chung, Y. J. Li, R. M. Ho, B. T. Ko, U. S. Jeng, and B. Lotz, *Macromolecules*, **39**, 5782 (2006).
25. S. Nojima, Y. Akutsu, A. Washino, and S. Tanimoto, *Polymer*, **45**, 7317 (2004).
26. S. Nojima, Y. Akutsu, M. Akaba, and S. Tanimoto, *Polymer*, **46**, 4060 (2005).
27. S. Nojima, K. Ito, and H. Ikeda, *Polymer*, **48**, 3607 (2007).
28. V. Crescenzi, G. Manzini, G. Calzolari, and C. Borri, *Eur. Polym. J.*, **8**, 449 (1972).
29. S. Nojima, K. Kato, S. Yamamoto, and T. Ashida, *Macromolecules*, **25**, 2237 (1992).
30. S. Nojima, K. Hashizume, A. Rohadi, and S. Sasaki, *Polymer*, **38**, 2711 (1997).
31. S. Nojima, N. Kikuchi, A. Rohadi, S. Tanimoto, and S. Sasaki, *Macromolecules*, **32**, 3727 (1999).
32. M. Avrami, *J. Chem. Phys.*, **7**, 1103 (1939).
33. I. H. Hillier, *J. Polym. Sci., Part A*, **3**, 3067 (1965).
34. A. Booth and J. N. Hay, *Polymer*, **12**, 365 (1971).
35. S. Nojima, H. Nakano, Y. Takahashi, and T. Ashida, *Polymer*, **35**, 3479 (1994).
36. N. Sakamoto and T. Hashimoto, *Macromolecules*, **28**, 6825 (1995).
37. D. J. Quiram, R. A. Register, and G. R. Marchand, *Macromolecules*, **30**, 4551 (1997).
38. S. Nojima, M. Toei, S. Hara, S. Tanimoto, and S. Sasaki, *Polymer*, **43**, 4087 (2002).
39. J. Y. Hsu, I. F. Hsieh, B. Nandan, F. C. Chiu, J. H. Chen, U. S. Jeng, and H. L. Chen, *Macromolecules*, **40**, 5014 (2007).
40. Y. Chatani, Y. Okita, H. Tadokoro, and Y. Yamashita, *Polym. J.*, **1**, 555 (1970).

